BMC Oral Health

RESEARCH

Open Access

Real-time segmentation and detection of ponticulus posticus in lateral cephalometric radiographs using YOLOv8: a step towards enhanced clinical evaluation

Mehmet Akyuz[1], Seyda Besnili[2], Guldane Magat[3*] and Murat Ceylan[4]

Abstract

Objectives Ponticulus posticus (PP) is a bony structure in the cervical spine, often difficult to identify in radiographic images, and its detection is important for both orthodontic diagnosis and clinical decision-making related to craniovertebral pathologies. The purpose of this study is to develop a deep learning-based approach for detecting the PP in lateral cephalometric radiographs using the YOLOv8-seg model.

Methods This retrospective study analyzed a dataset of 1000 anonymized lateral cephalometric radiographs, focusing on the segmentation and detection of the PP. Images were resized to 640 × 640 pixels and labeled by two experienced dentomaxillofacial radiologists. The YOLOv8-seg model, designed for segmentation tasks, was trained over 100 epochs with a batch size of sixteen, using pre-trained weights from the COCO dataset. Model performance was evaluated using precision, recall, mean average precision (mAP), and F1 score metrics.

Results The YOLOv8s-seg model demonstrated high accuracy in detecting the PP, with a precision of 62.81%, recall of 88.7%, mAP50 of 75.27%, mAP95 of 62.28%, and an F1 score of 73.54%. Even in cases where the boundaries of the C1 cervical vertebra were not clearly distinguishable, the model performed effectively, suggesting its reliability in clinical applications.

Conclusions The proposed YOLOv8-seg model shows promising potential for improving the accuracy and efficiency of PP detection in lateral cephalometric radiographs. By integrating AI into the diagnostic process, orthodontic practices can benefit from more precise and reliable identification of small but clinically significant anatomical structures, ultimately enhancing patient care and diagnostic accuracy.

Keywords Deep learning, Lateral cephalometric radiographs, Ponticulus posticus, YOLOv8-seg model, Orthodontic diagnosis

*Correspondence:
Guldane Magat
gul_dent@hotmail.com
[1]Oral and Maxillofacial Radiologist, Denizli Oral and Dental Health Center, Denizli, Türkiye
[2]Software Engineer at a Private Company, Konya, Türkiye
[3]Faculty of Dentistry, Department of Oral and Maxillofacial Radiology, Necmettin Erbakan University, Konya, Türkiye
[4]Faculty of Engineering and Natural Sciences, Department of Electrical and Electronics Engineering, Konya Technical University, Konya, Türkiye

Introduction

The cervical vertebrae of the human spine exhibit considerable anatomical variability, particularly the first cervical vertebra, the Atlas [1]. Unique in structure, the Atlas lacks a body and spine, distinguishing it as the most variable vertebra. Its posterior arch plays a critical role in clinical conditions associated with the craniovertebral junction [2]. Structurally, the Atlas consists of anterior and posterior arches, lateral masses, and transverse processes, with its superior articular facets forming the atlanto-occipital joint, a region prone to various anatomical variations [3].

One such variation is the ponticulus posticus (PP), a small bony bridge that connects the superior articular process to the superior margin of the posterior arch. Also referred to as the dorsal ponticle or arcuate foramen, the PP has significant clinical implications, particularly due to its potential compression of the vertebral artery, which can lead to symptoms such as headaches and vertigo [4]. Theories regarding its formation include ligament ossification due to aging and adaptive responses to craniocervical dynamics [2]. Clinically, the PP is implicated in conditions such as migraines, neck and shoulder pain, and a group of symptoms collectively referred to as "Upper Cervical Syndrome," which includes dizziness, visual disturbances, tinnitus, and cervicogenic headaches resulting from dysfunction or compression at the craniocervical junction [5, 6]. Despite not being a primary focus in orthodontics, its detection on lateral cephalometric radiographs (LCRs) is crucial for potential neurological referrals [7]. Reported prevalence rates vary significantly (4.3-46.0%) across different populations [8]. Additionally, the bony protrusion formed by the PP may lead to biomechanical changes in the upper cervical spine, potentially increasing the risk of odontoid fractures [9].

LCRs are routinely used in orthodontics for various diagnostic purposes, including age estimation, assessment of skeletal and dental relationships, growth pattern analysis, and treatment planning for dentofacial anomalies [10]. However, manual interpretation of these radiographs is often time-consuming and prone to interobserver variability. Recent advances in artificial intelligence (AI), particularly machine learning and deep learning algorithms, have demonstrated significant potential in improving detection accuracy and efficiency. AI models can analyze LCRs with high precision and consistency, detecting subtle anatomical variations such as PP, which may often be overlooked in routine clinical assessments [11–13].

Among AI-driven detection models, the You Only Look Once (YOLO) model has gained prominence for its real-time object detection capabilities, processing images in a single pass to achieve high efficiency [14, 15]. Since its introduction in 2016, YOLO has evolved from YOLOv1 to YOLOv12, with each iteration improving speed, accuracy, and computational efficiency [14, 16]. Unlike multi-stage models like Faster R-CNN, which involve separate region proposal and classification steps, YOLO operates as a single regression-based framework, predicting bounding boxes and class probabilities simultaneously [14, 17]. Due to these advantages, YOLO has been widely applied in autonomous systems, industrial automation, medical imaging, and dentistry [18, 19]. In dental radiology, YOLO-based models have been successfully implemented for automated cephalometric landmark detection, dental caries identification, and panoramic radiograph analysis, enhancing diagnostic accuracy and workflow efficiency [20, 21]. Recent developments, such as YOLOv8-seg, integrate segmentation and detection, enabling precise localization of anatomical structures [16].

This study aims to evaluate the performance of the YOLOv8-seg model for simultaneous segmentation and detection of PP in LCRs, assessing its potential to enhance AI-assisted orthodontic diagnostics. To the best of our knowledge, no prior computer-assisted approach has been specifically developed for the detailed assessment of PP in the first cervical vertebra, leaving this field largely unexplored. By leveraging AI based on convolutional neural networks (CNNs), we aim to improve PP identification in lateral cephalograms, a structure often overlooked due to its small size and complex anatomical surroundings. This study seeks to establish a new standard in orthodontic diagnostics, demonstrating AI's superiority in detecting anatomical anomalies and ultimately enhancing craniofacial examination accuracy and efficiency.

Material and method

Data

Ethical statement

The study was approved by the Ethics Committee of Necmettin Erbakan University Faculty of Dentistry Pharmaceutical and Non-Medical Device Research Ethics Committee (Approval Number: 09-154/1). Written informed consent to participate was obtained from all participants included in the study.

Post hoc power analysis

To evaluate the statistical sensitivity of the model performance, a post hoc power analysis was conducted using G*Power 3.1 software (Düsseldorf, Germany). The analysis was based on the observed recall value (0.887) in the test set ($n = 100$), assuming a baseline proportion of 0.5 and a significance level of 0.05. The computed effect size was entered into a two-tailed test for the difference between two independent proportions. The resulting statistical power was 0.9999, indicating a very high

probability of correctly detecting a true effect and supporting the adequacy of the sample size for evaluating the model's diagnostic performance.

Subjects

In this retrospective study conducted at Necmettin Erbakan University, Faculty of Dentistry, Turkey, pretreatment lateral cephalometric radiographs (LCRs) of patients requesting orthodontic treatment, were evaluated. The study included a comprehensive review of LCRs previously collected for orthodontic diagnosis, excluding those with incomplete documentation, a history of syndromic or systemic disease, a history of dentofacial trauma, presence of the cervical vertebrae malformation, or poor-quality radiographs, especially unclear cervical spine images. Each radiograph was captured using the J MORITA (2D Veraviewpocs, MFG corp, Kyoto, Japan) system. The settings for these images were consistent: a tube voltage of 65 kV, a tube current of 10 mA, and an exposure duration of 4.9 s. The procedures for taking these radiographs adhered strictly to the guidelines provided by the manufacturer. According to these criteria, a total of 783 individuals were included in the study.

Preparation of the input data and ground truth

LCRs with resolutions of 1750×1537, 1024×899, 1024×798 or 1024×949 pixels were collected, clearly showing the cervical vertebrae, especially C1, C2, C3 and C4. LCRs were exported in JPEG format for further processing. The acquired images were fully anonymized to ensure confidentiality and ethical compliance. The boundaries of the C1 cervical vertebra were meticulously marked on all radiographs by two dentomaxillofacial radiologists (G.M. and M.A.), with 14 and 4 years of experience, respectively. Ground truth labeling of PP in radiographs was conducted using the VGG Image Annotator (VIA) Labeling Tool (developed by the Visual Geometry Group, University of Oxford, UK) on an open-source labeling platform. A consensus-based approach was applied for each annotation using the polygonal box method. Radiographs lacking unanimous agreement were excluded from the study. The classification of PP was categorized into three groups: none, partial, or complete.

Method

YOLOv8 architecture

Since its introduction by Ultralytics in 2022, YOLOv8 has become a frequently used object detection architecture for medical applications (Fig. 1a). The YOLOv8-Seg model, designed for segmentation tasks, is an extension of the YOLOv8 object detection architecture. YOLOv8-Seg is a single-shot architecture that performs pixel-wise segmentation of objects of interest in an image and estimates their class probabilities. The YOLOv8 model consists of 3 parts: the backbone used for feature extraction, the neck that combines feature maps from different layers, and the head that generates the result. These parts are analyzed and introduced under separate headings.

Backbone

In YOLOv8, CSPDarkNet53 is used as the default backbone. This backbone is a pre-trained convolutional neural network (CNN) [22] responsible for extracting feature maps at different levels from the input image. CSPDarkNet53 improves DarkNet-53 by adding the Cross Stage Partial Connections (CSP) feature [23]. CSPDarkNet53 uses a CSPNet strategy to divide the base layer's feature map into two parts and then combine them through a cross-phase hierarchy. The use of a divide-and-conjoin strategy allows more gradients to flow through the network [24]. This increases the generalization capability of the model while reducing the computational cost. Unlike previous YOLO models, YOLOv8 introduces the C2f module, which enhances gradient flow and improves feature extraction efficiency. The C2f module consists of two convolutional layers and n (the number of bottlenecks) DarknetBottleneck layers, which are interconnected through Split and Concat operations. The convolution modules here consist of Conv-BN-SiLU [25]. At the end of the backbone, a spatial pyramid pooling layer (SPPF) is used to aggregate the feature maps of different sizes obtained from the convolution layers (Fig. 1b).

Neck

Mechanisms such as feature pyramid networks (FPN) or path aggregation networks (PAN) provide additional layers and mechanisms to improve features. YOLOv8 combined the two to improve feature fusion capability at the neck. Deep neural networks provide more detailed information for smaller objects in the lower layers of feature extractors, while the upper layers provide more general information for larger objects. FPN has strong top-down semantic properties, while PAN has strong bottom-up localization properties [26]. PAN-FPN establishes a bidirectional network structure that integrates top-down and bottom-up pathways, enabling the fusion of shallow spatial details with deep semantic features. This fusion enhances feature diversity and completeness, ensuring a more comprehensive representation of the data (Fig. 1c) [27].

Head

The head part processes the data patterns from the previous layers to produce the result. The head is designed to be split into two branches to reduce the conflict between localization and classification. These heads are used to estimate segmentation masks for each object. It typically applies a pixel-wise classification by expanding the

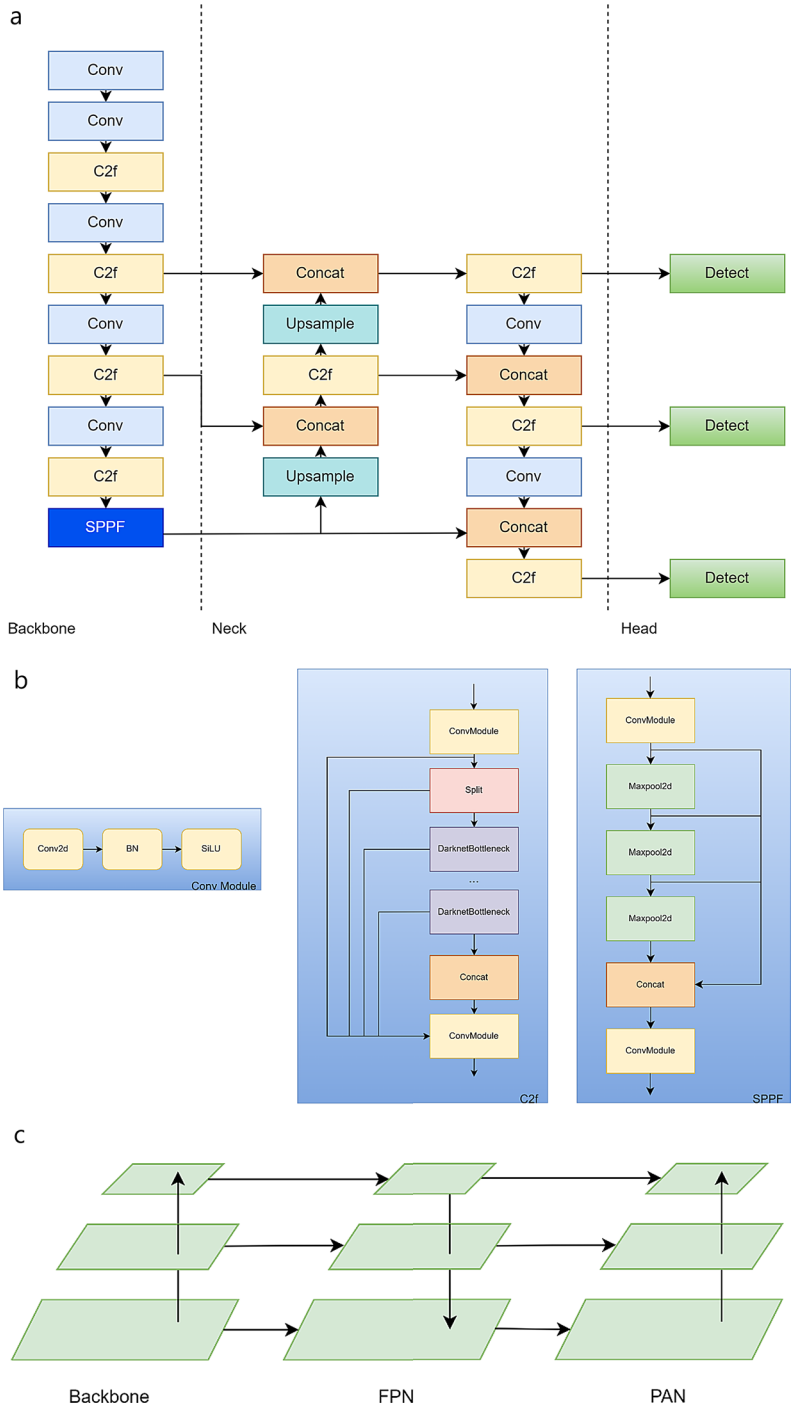

Fig. 1 (**a**) YOLOv8 architecture, (**b**) Conv, C2f, and SPPF modules, (**c**) FPN and PAN mechanisms

feature maps to the original image size and using a set of convolutional layers to determine to which class each pixel belongs (Fig. 2).

Loss

Classification uses binary cross entropy (BCE) loss, while bounding box regression uses distribution focal loss (DFL) and complete IoU (CIoU). The weighted sum of these losses forms the final loss used to train the model. Equation 1:

$$Loss = BCE\ Loss + CIoU\ Loss + DFL \quad (1)$$

The hyperparameters 'cls', 'dfl' and 'box' are used to increase the importance of the loss functions according to the task. The default values of 1.5, 0.5 and 7.5 were set

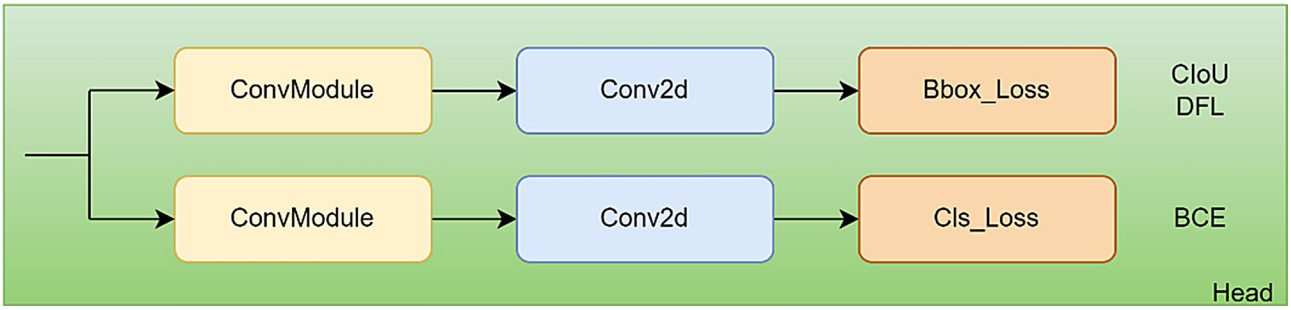

Fig. 2 Head module

to 2 (cls), 0.5 (dfl) and 7.5 (box), respectively, as a result of the experimental study to increase the focus on PP classification, which is the main objective of this study.

BCE loss calculates the loss for each pixel, taking into account the predicted class probabilities and the actual labels. It then averages the losses of all pixels. The Cross Entropy Loss (BCE) is shown in Eq. 2:

$$BCE\ Loss = -w_n[y_n \cdot\ logx_n + (1 - y_n) \cdot\ log(1 - x_n)] \quad (2)$$

Where w_n is the weight value, y_n is the labeled value and x_n is the prediction value of the model. When there are too few instances of a particular object class in the training set, i.e. when there is an imbalance between the total number of instances representing each class, the network often struggles to learn to correctly detect objects. Distribution focal loss (DFL) helps to improve the performance of the model by giving more importance to classes with fewer instances in cases of class imbalance. DFL basically aims to model the location of the target box as a general distribution and increase its probabilities by allowing the network to focus faster on values close to the target location [28]. DFL considers the location of the target box as a general distribution (not just as a single point, but with other points close to that point). This requires the use of linear interpolation to weight the distance between integer coordinates. This weighting ensures that more importance is given to locations that are closer to the actual position of the target box, thus helping the model to more accurately predict the actual positions of objects. Distribution focal loss (DFL) is shown in Eq. 3:

$$\begin{aligned} DFL(S_i\ ,\ S_i + 1)\ =\ &-((\ y_{i+1} -\ y)\, loglog\ (S_i) \\ &+ (y\ -\ y_i)\ log\,(S_{i+1})) \end{aligned} \quad (3)$$

Where S_i and S_i+1 represent the score of two consecutive predictions and y-values represent their true labels. IoU (Intersection over Union) quantifies the overlap between the predicted bounding box and the actual bounding box. A value of 1 indicates a perfect overlap, while an IoU of 0 signifies no intersection between the two boxes. IoU is shown in Eq. 4:

$$IoU = \frac{|\,A \cap\ B|}{|A| \cup\ |B|} \quad (4)$$

The terms A and B in Eq. 4 refer to the predicted and actual positions of the two objects. CIoU takes into account the aspect ratios between the boundaries in addition to the overlap between the loss prediction and the actual label. Eq. 55:

$$CIoU = 1 - IoU\ +\ \frac{Distance_2^2}{Distance_C^2} + \frac{v^{\,2}}{(1 - IoU) + v} \quad (5)$$

The term v in Eq. 5 refers to the difference between the size of the boxes (aspect ratio).

ProtoNet

The YOLOv8-Seg model shares the same basic architecture as the YOLOv8 object detection architecture. The difference is that there is an additional layer in the head, ProtoNet, which generates the mask coefficients (Fig. 3).

ProtoNet is implemented as a fully convolutional neural network (FCN) that estimates k prototype masks for the whole image. This neural network has k channels in its last layer (one channel for each prototype) and is added to a backbone feature layer. ProtoNet takes as input the P3 feature map, which is rich in resolution and spatial information [29]. ProtoNet improves the overall performance of multiclass segmentation by providing more accurate prediction-label overlap and more accurate classification results.

Post-estimation

After model estimation, non-maximum suppression (NMS) is used to improve the outputs and remove duplicate detections. NMS is a frequently used post-processing method in object detection. During estimation, there may be overlapping or very close masks produced by the model. In this case, it is used to clean multiple masks representing the same object. NMS basically ranks all

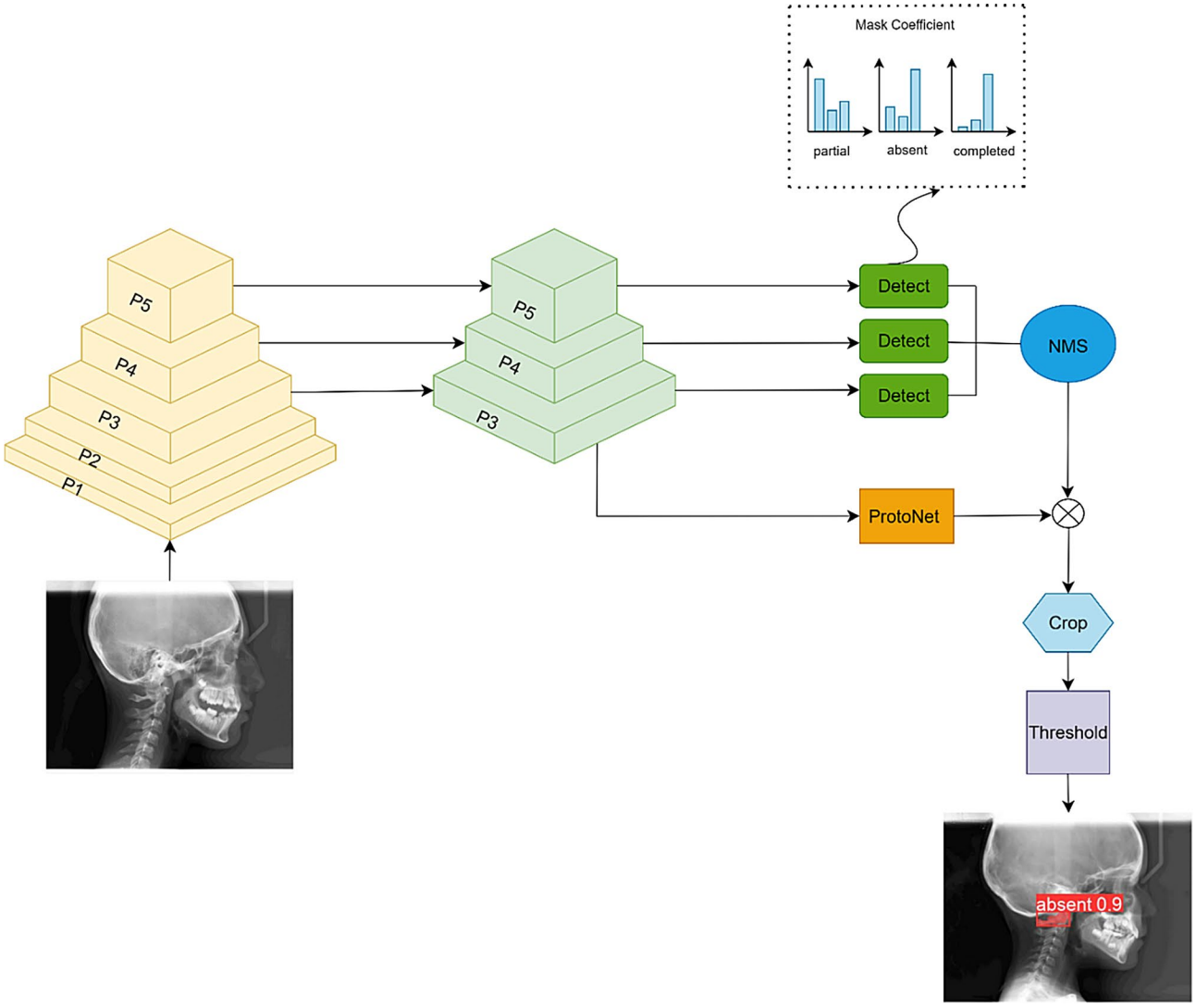

Fig. 3 YOLOv8 architecture extended with ProtoNet convolutional neural network

predictions according to a confidence score. Then, the detection with the highest confidence score is compared with other detections representing the same object using a certain threshold of overlap (Intersection over Union - IoU). Thresholding steps are applied to filter out predictions with low confidence. In this way, the detections with the highest confidence score remain.

Data augmentation

The dataset contains a total of 1000 original images, 800 images belonging to the absent class, 100 images belonging to the partial class and 100 images belonging to the completed class. The images constituting the dataset were taken from more than one shooting device, which causes heterogeneity in the dataset. In order to reduce the effect of heterogeneity in the dataset on model performance, data augmentation techniques such as hsv_h, hsv_s, hsv_v, translate, flipr were applied to the input data to increase the data. Another data augmentation technique used during training is mosaic data augmentation (Fig. 4*).* Mosaic data augmentation involves combining, resizing, and merging multiple images into a single image to create new contexts that the model can learn from. In this way, the complexity of the training data increases, and since the model sees multiple images as a randomly combined single image, its generalization ability improves.

Training configuration

For network training, a 12th Generation Intel(R) Core (TM) i7-12800HX processor was used. The models were trained over 100 epochs with a batch size of sixteen. The pre-trained weights of the model trained on the COCO dataset were utilized. Adam (Adaptive Moment Estimation) was employed as the optimization algorithm. Adam uses adaptive learning to improve gradient descent,

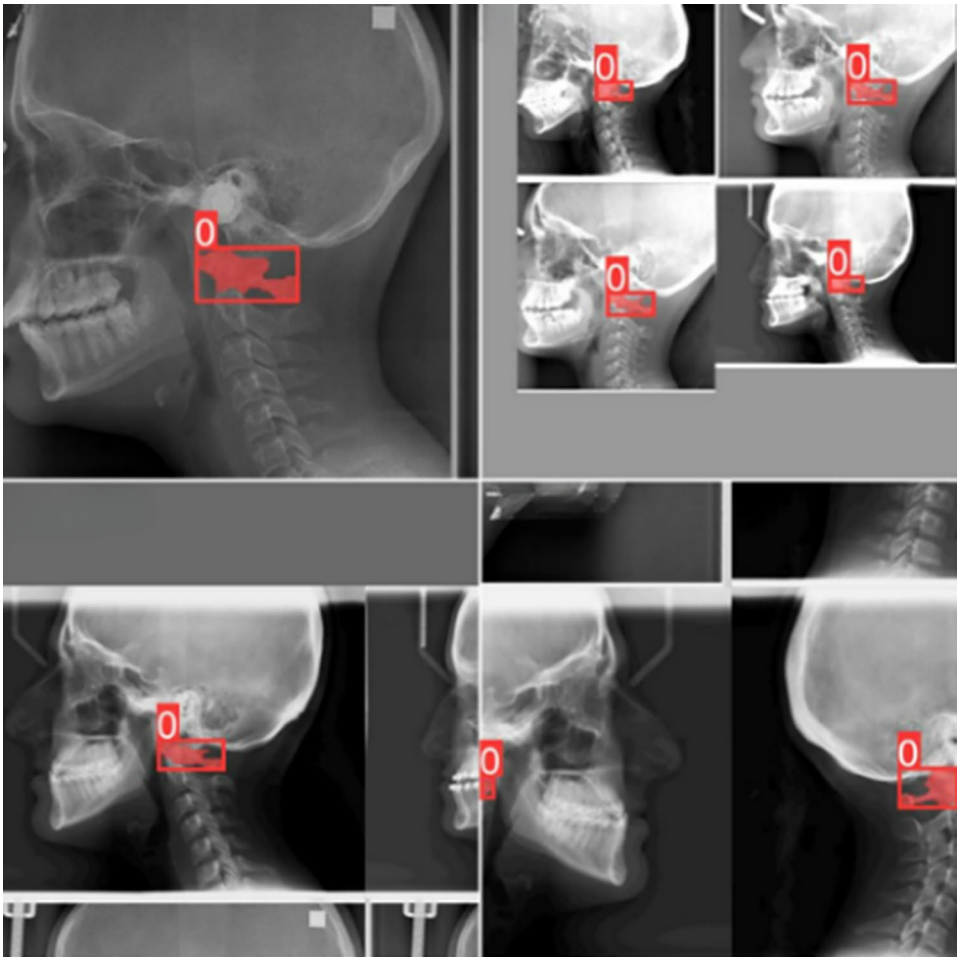

Fig. 4 Training images augmented with mosaic data augmentation technique

which typically results in faster and more effective convergence, especially when working with complex models [30]. Lateral cephalograms were resized to 640 × 640 dimensions. The number of worker threads for data loading was set to 8. The model weights were adjusted using a learning rate of 0.01. To enhance learning efficiency and avoid local minima, a momentum value of 0.937 was applied. To prevent overfitting, the weight decay was adjusted to 0.0005. All procedures were carried out using PyCharm 2021.3.1 (JetBrains, Prague, Czech Republic). Python (version: 3.10.1), an open-source programming language, was used to develop an AI model for PP segmentation. A total of 1000 anonymized cephalometric images of varying sizes were used, and the images were divided into three categories for training, validation, and testing (Fig. 5):

Training group: 700 (700 labels).
Validation group: 200 (200 labels).
Test group: 100.

Performance evaluation

The performance of the models was evaluated using precision, recall, mAP50, mAP95, and F1 metrics. The parameters used to calculate precision and recall are TP (True Positive), FP (False Positive), and FN (False Negative):

- **TP (True Positive)**: Represents examples that are predicted as positive and are indeed positive.
- **FP (False Positive)**: Represents examples that are predicted as positive but are actually negative.
- **FN (False Negative)**: Represents examples that are predicted as negative but are actually positive.
- **Precision** shows the ratio of true positives within the total predicted positives. A high precision value indicates that the model has a high likelihood of correctly identifying positive examples among those it predicts as positive. Equation 6:

$$Precision = \frac{TP}{TP + FP} \tag{6}$$

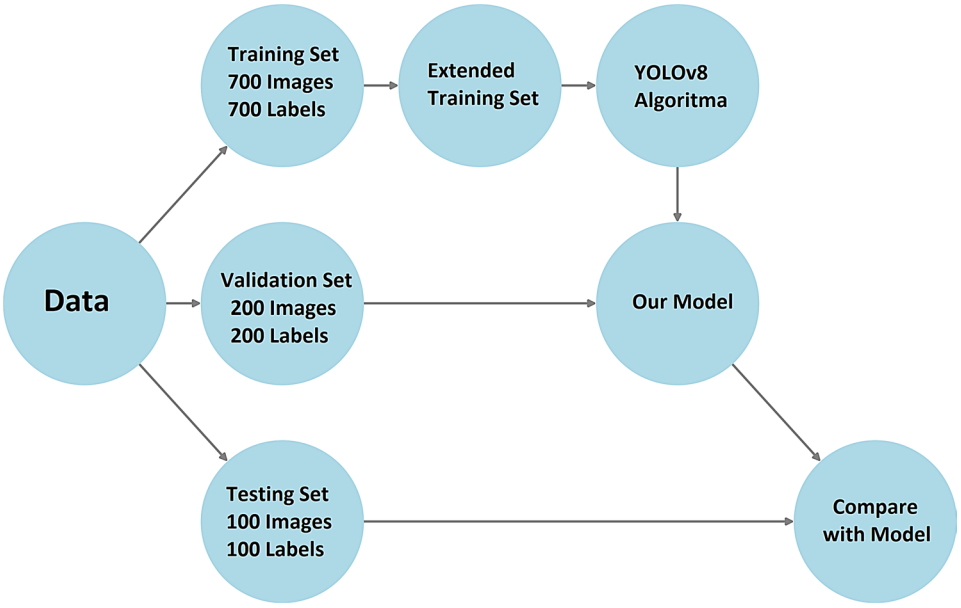

Fig. 5 Flowchart of the model development process

- **Recall** (or sensitivity) shows the ratio of true positives within the total actual positives. A high recall value indicates that the model is sensitive and does not miss many actual positive examples. Equation 7:

$$Recall = \frac{TP}{TP + FN} \tag{7}$$

- **Average Precision (AP)** produces a single value representing the model's performance by calculating the area under the precision-recall curve. Equation 8:

$$AP = \int_0^1 Precision\ (Recall)\ d\,(Recall) \tag{8}$$

- **Mean Average Precision (mAP)** extends the concept of AP by calculating the AP for all classes and then averaging them. This provides an overall metric to evaluate the model's performance across all categories. mAP50 refers to the mean AP calculated at a single Intersection over Union (IoU) threshold of 0.50, indicating a more lenient overlap requirement between predicted and ground truth bounding boxes. mAP95 represents the average of AP values computed at multiple IoU thresholds ranging from 0.50 to 0.95 in steps of 0.05. This metric provides a more stringent and comprehensive assessment of the model's detection accuracy across different levels of localization precision. Equation 9:

$$mAP = \frac{1}{N} \sum {}_{i=1}^{N} APi \tag{9}$$

- The **F1 score** represents the harmonic mean of the precision and recall metrics. A high F1 score indicates that the model minimizes both false positives and false negatives, demonstrating that the model has generally good overall performance. Equation 10:

$$F1 = \frac{2 \times\ Precision \times\ Recall}{Precision + Recall} \tag{10}$$

YOLOv8 offers five different models based on the number of parameters: nano, small, medium, large, and extra-large. The nano model is the smallest and lightest, with fewer parameters and lower computational cost. The extra-large model has the most parameters and the most complex architecture, making it the model with the highest computational cost to achieve the highest accuracy and performance. All other models fall between these two in terms of parameter count and computational cost (Table 1).

Results

In this study, the proposed method for detecting PP in LCRs was developed using YOLOv8-seg models. Among the tested architectures, the YOLOv8s-seg model showed the strongest detection sensitivity, achieving the highest recall (0.8870) and mAP50 (0.7527). While its precision (0.6281) was lower compared to other models, the high recall value indicates that the model successfully detected truest positive cases. In contrast, the YOLOv8m-seg and YOLOv8l-seg models demonstrated more balanced performances. Specifically, YOLOv8m-seg yielded the highest F1-score (0.7435), reflecting a good compromise

Table 1 YOLOv8 segmentation models and parameter values

Model	Size (pixels)	mAPbox (50–95)	mAPmask (50–95)	Speed CPU ONNX(ms)	Speed A100 TensorRT(ms)	Params(M)	FLOPs(B)
YOLOv8n-seg	640	36.7	30.5	96.1	1.21	3.4	12.6
YOLOv8s -seg	640	44.6	36.8	155.7	1.47	11.8	42.6
YOLOv8m-seg	640	49.9	40.8	317.0	2.18	27.3	110.2
YOLOv8l -seg	640	52.3	42.6	572.4	2.79	46.0	220.5
YOLOv8x-seg	640	53.4	43.4	712.1	4.02	71.8	344.1

Table 2 Performance of YOLOv8 segmentation models on the lateral cephalometric radiograph dataset at 100 epochs

Model	Precision	Recall	mAP50	mAP95	F1
YOLOv8n-seg	0.7198	0.6917	0.72022	0.58991	0.7054
YOLOv8s-seg	0.6281	0.8870	0.7527	0.6228	0.7354
YOLOv8m-seg	0.6694	0.8363	0.7167	0.5954	0.7435
YOLOv8l-seg	0.6506	0.8389	0.7291	0.6011	0.7328

between precision and recall, while YOLOv8l-seg showed comparable performance with an F1-score of 0.7328 and competitive mAP values. These results are summarized in Table 2. To support these findings visually, Figs. 6, 7, and 8 present representative segmentation results generated by the YOLOv8s-seg model. Figure 6 illustrates successful detections in cases with clearly defined PP morphology. Figure 7 presents the confusion matrix for the model's predictions, illustrating its classification performance across categories. Figure 8 illustrates borderline cases with partially visible PP, highlighting the model's robustness in scenarios that may challenge human interpretation.

Discussion

This study was conducted to address a significant gap in the assessment of the PP in the first cervical vertebra, which is often overlooked in orthodontic diagnostics due to its small size and complex surroundings. Despite advancements in imaging techniques, the detailed evaluation of the PP has not been adequately explored, leading to potential misdiagnoses. By leveraging AI, specifically the YOLOv8s-seg model, this research aims to enhance the detection of the PP in LCRs. The motivation behind

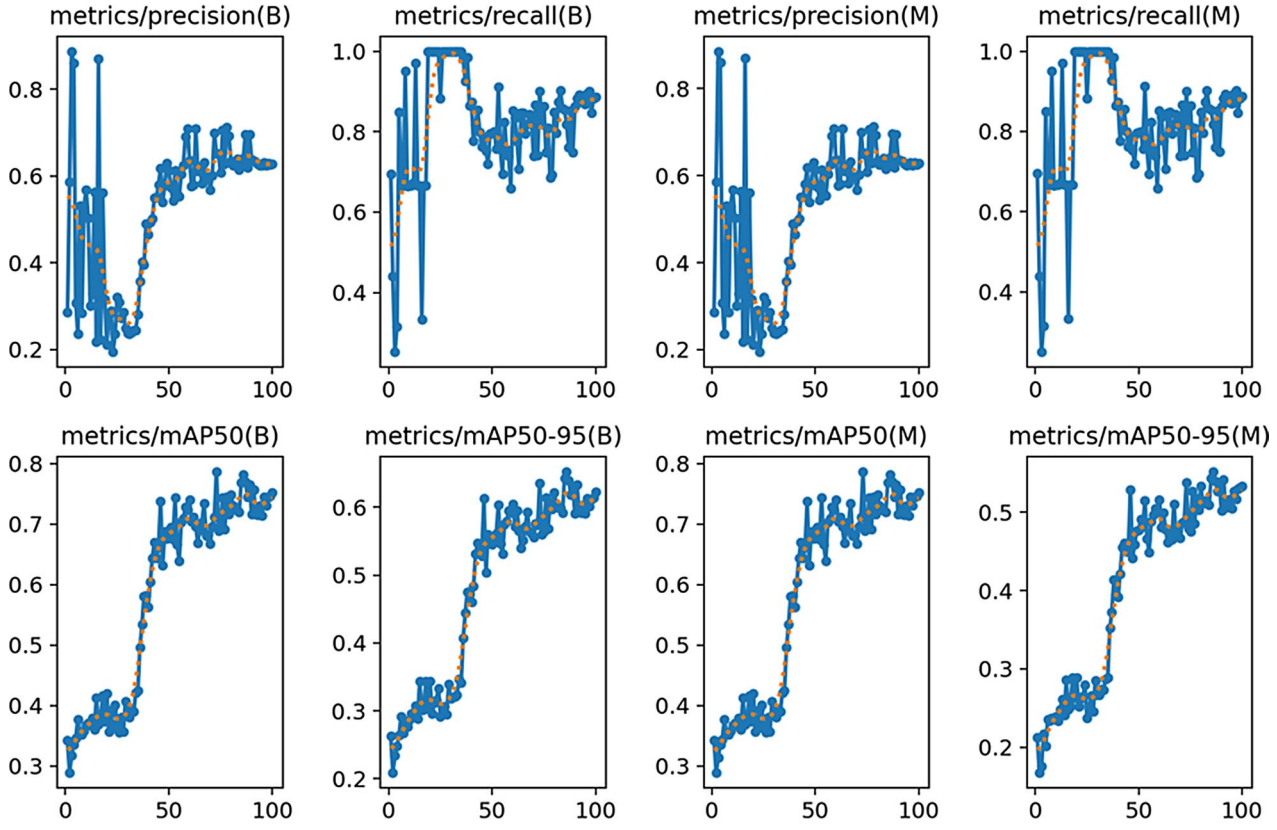

Fig. 6 Result graphs of YOLOv8s-seg model

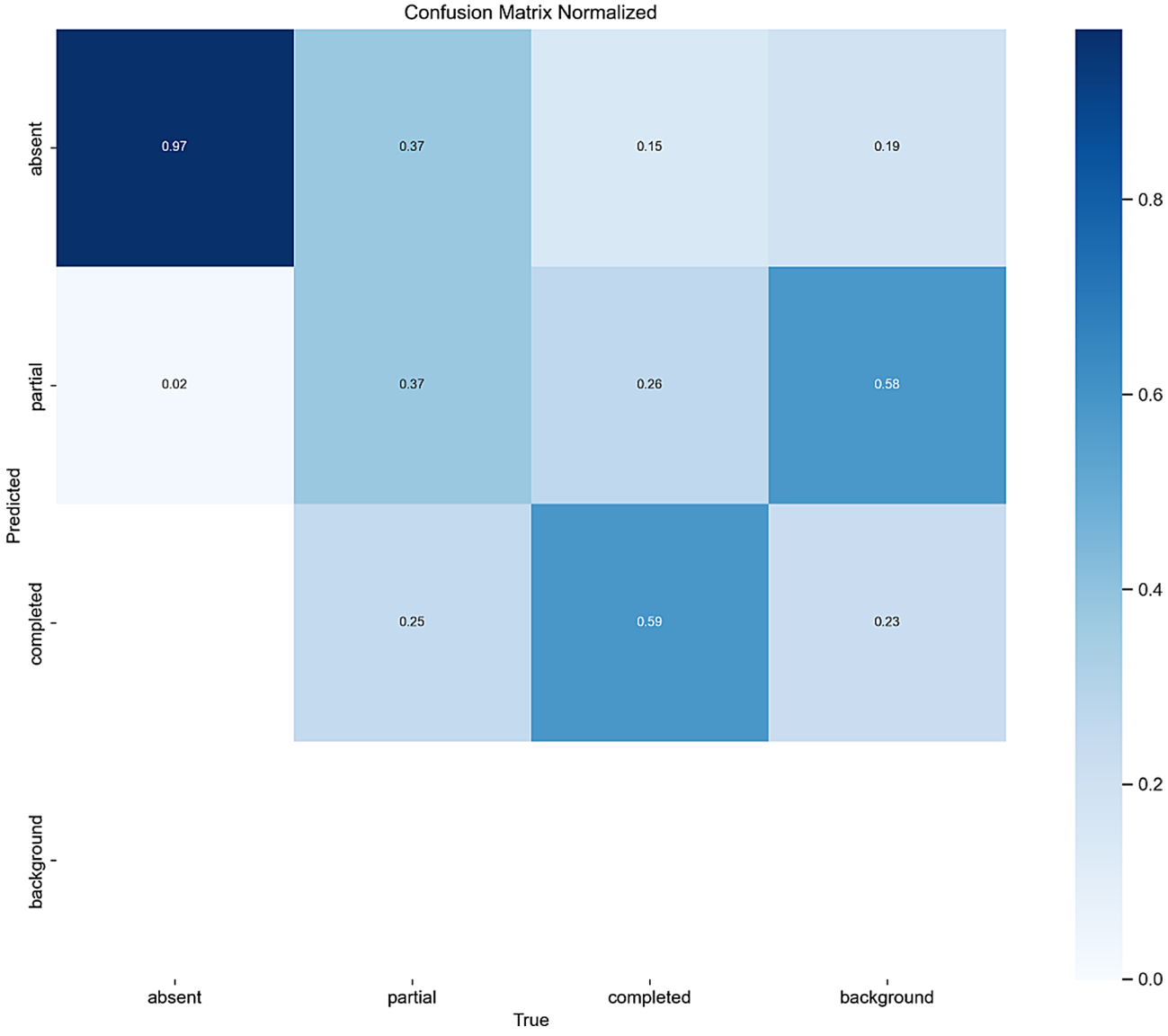

Fig. 7 Confusion matrix of the YOLOv8s-seg model on the validation dataset

this study is to improve diagnostic accuracy and efficiency in orthodontics, ultimately establishing a new standard for craniofacial examinations and enhancing patient outcomes in this underexplored area.

The integration of AI algorithms in the analysis of LCRs holds great promise for enhancing treatment planning in orthodontics by facilitating quicker and more precise diagnoses. Prior studies have demonstrated the efficacy of AI in identifying intricate anatomical features, and our research further confirms that even subtle and frequently neglected anomalies, such as the PP, can be effectively detected [31, 32]. Given that the presence of PP has been clinically linked to various symptoms, including migraines, headaches, and vertigo, its accurate identification is crucial for informing treatment strategies and improving patient care [33]. By harnessing the capabilities of AI, orthodontists can ensure that such significant anatomical variations are not overlooked, ultimately contributing to more comprehensive and effective treatment plans for their patients.

The YOLOv8 algorithm used in PP segmentation-detection offers significant advantages compared to other object detection algorithms. The single-step detection architecture provides improvements in both speed and accuracy. While traditional methods usually follow a multi-step process, YOLOv8 performs all operations in a single pass, which is valuable for real-time diagnosis and analysis in clinical settings [34–36]. YOLOv8 also enhances model performance by ensuring better gradient flow through its CSPDarkNet53 backbone, which efficiently combines multi-level feature maps—an essential feature for accurately identifying small anatomical

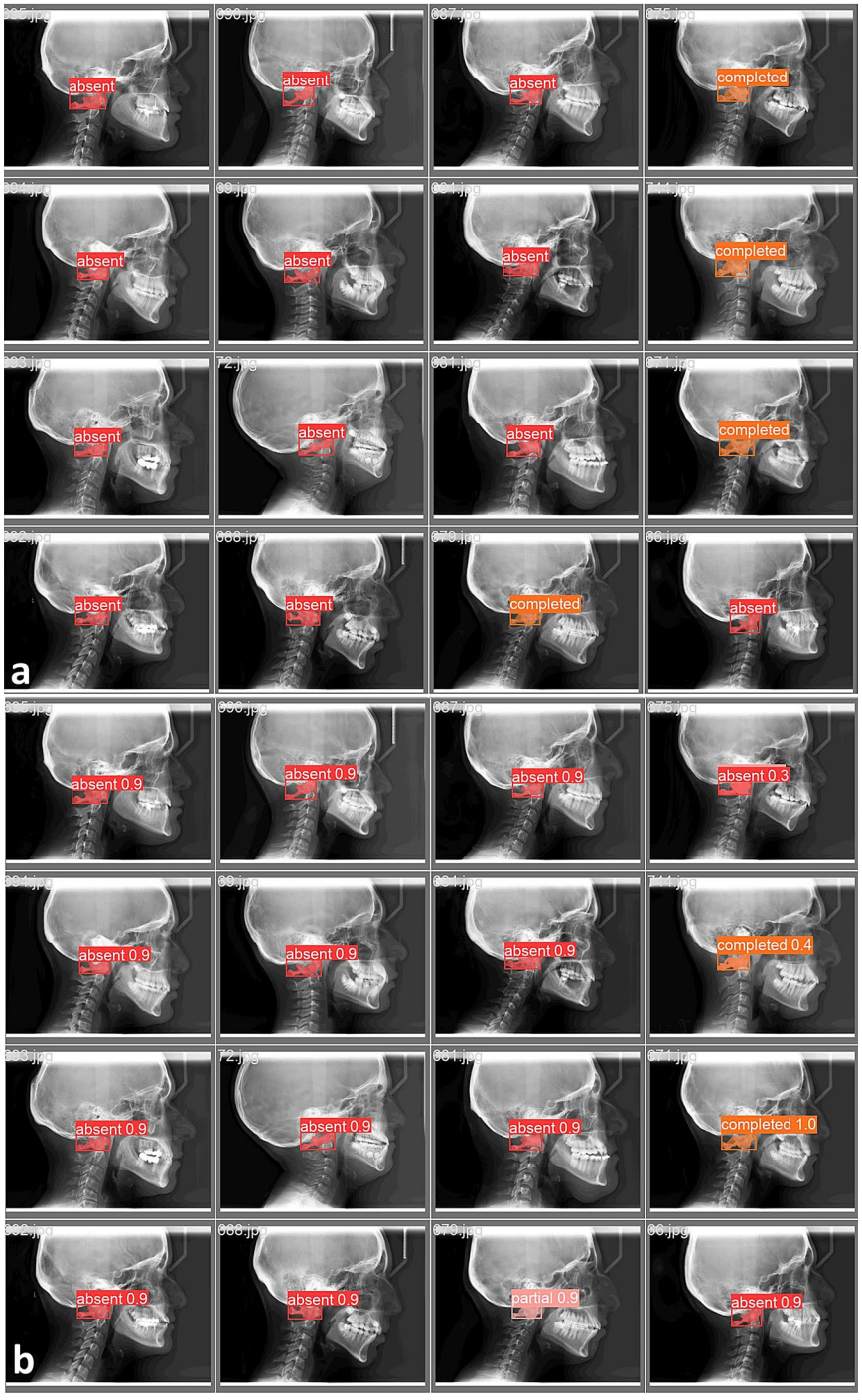

Fig. 8 Examples of absent, partial, and completed detection in the validation dataset. (**a**) manually labeled images, (**b**) predicted images

structures such as the PP, which are often obscured or difficult to localize. Additionally, the C2f module and FPN/PAN feature pyramid networks integrated into YOLOv8 allow the model to extract robust multi-scale features, thereby supporting effective detection of both small and large objects [37, 38]. The lack of such enhancements in earlier versions or other frameworks makes it more challenging to detect rare and morphologically variable structures like the PP. Furthermore, although newer versions in the YOLO family (e.g., YOLOv9 and beyond) have since been announced, YOLOv8 represented the most stable and fully documented version available at the time of model development, and importantly, it offered native segmentation support through the YOLOv8-seg framework. Unlike newer iterations that were still undergoing refinement or lacked official segmentation

modules, YOLOv8-seg provided a robust and reproducible platform for our dual objective: simultaneous detection and segmentation. Its technical maturity, widespread adoption, and active development community also facilitated implementation in a clinical research context [39, 40]. Therefore, YOLOv8 was considered the most appropriate version for our study's goals and timeframe.

During model development, the dataset included LCRs of varying native resolutions (e.g., 1750 × 1537, 1024 × 899, 1024 × 798, and 1024 × 949 pixels). Although differences in image resolution can theoretically affect feature consistency across samples, all images in this study were uniformly resized during preprocessing to ensure compatibility with the model input requirements—a standard approach in convolutional neural network-based workflows [41]. Furthermore, the YOLOv8-seg architecture leverages advanced design components such as C2f modules and spatial pyramid pooling, which are engineered to extract robust multi-scale features and improve model resilience to scale variations [24]. These components help maintain detection accuracy even when the resolution of the original images varies [42], supporting the reliability of the results obtained across heterogeneous input dimensions.

The advantages of the YOLO family of models include their efficiency in balancing speed and accuracy, making them particularly well-suited for real-time detection and segmentation tasks. YOLO models operate as a single regression problem, significantly reducing detection time compared to earlier frameworks like R-CNN and Single Shot Detector (SSD) [43]. Among the YOLO series, YOLOv7 has been recognized for its enhanced accuracy while maintaining fast inference speeds [44], and lightweight variants such as YOLO-Banana have demonstrated efficient detection capabilities in specialized applications [45]. In our study, YOLOv8-seg was utilized to detect and segment the PP in LCRs, leveraging these advantages for accurate landmark identification in orthodontics. However, despite these benefits, YOLO-based models, including YOLOv8-seg, are known to face challenges in small object detection. Studies indicate that one-stage models like YOLO and two-stage models such as Faster R-CNN struggle with detecting small anatomical structures due to a lack of distinguishing features, the influence of surrounding anatomical noise, and feature loss in deeper layers of convolutional networks caused by pooling and normalization operations [19, 46]. This limitation is relevant to our study, as precisely segmenting and detecting the PP in lateral cephalograms presents similar difficulties, particularly in cases where the C1 vertebra boundary is indistinct or obscured by overlapping structures. Additionally, while YOLO models prioritize real-time processing, this speed can sometimes lead to a trade-off in accuracy, particularly when detecting complex or overlapping anatomical structures. In our study, the YOLOv8s-seg model achieved a high recall (88.7%), ensuring sensitivity in PP detection; however, its precision was relatively lower (62.81%), indicating an increased false-positive rate. This aligns with findings in other real-time applications where YOLO models may generate false positives and missed detections when handling minor or closely spaced objects [47, 48]. These challenges highlight the need for further optimization, particularly for small and overlapping structures in medical imaging tasks. In conclusion, while YOLOv8-seg demonstrated strong segmentation and detection capabilities in our study, addressing the inherent limitations of YOLO models in small object detection remains an important avenue for improvement. Future enhancements, such as multi-scale feature fusion, attention mechanisms, and specialized preprocessing techniques, could further improve YOLOv8-seg's performance in cephalometric landmark analysis and other medical applications, ensuring greater accuracy across a broader range of clinical detection tasks.

As shown in Table 2, performance metrics of the YOLOv8-seg model, such as 62.81% precision, 88.7% recall, 75.27% mAP50, 62.28% mAP95, and 73.54% F1 score, reflect its ability to accurately detect and segment the PP in LCRs [49, 50]. However, its precision (0.6281) was lower compared to other models, suggesting a higher rate of false positives. In contrast, YOLOv8l-seg exhibited a more balanced performance across all metrics, achieving a relatively high mAP50 (0.7291) and F1-score (0.7328), making it a strong candidate for accurate segmentation. The YOLOv8m-seg model showed slightly better precision than YOLOv8s-seg while maintaining a good recall, making it a compromise between the two approaches. Overall, the results suggest that model selection should be based on the trade-off between recall and precision, depending on the clinical application requirements. These findings align with previous research on deep learning applications in automated cephalometric landmark detection and analysis, though our study differs in that it employs a segmentation-detection model rather than a landmark classification-only approach. Lee et al. [51] utilized deep convolutional neural networks (DCNNs) such as Modified-AlexNet, MobileNet, and ResNet50 to classify cephalometric images and assess indications for orthognathic surgery based on maxillary and mandibular structures. Their approach focused on landmark detection and classification rather than full segmentation. Similarly, Zhao et al. [50]. investigated CNN-based automated adenoid hypertrophy detection, where the model identified key anatomical regions in lateral cephalograms for adenoid segmentation. Their study demonstrated high sensitivity (90.6%) and specificity (93.8%) in identifying adenoid hypertrophy, further

reinforcing the role of AI in cephalometric analysis. However, unlike our study, which integrates both segmentation and detection within a unified framework, their approach primarily focused on regional classification and segmentation rather than comprehensive object detection. These studies collectively support the efficacy of deep learning models in cephalometric analysis, but our work advances this field by utilizing a segmentation-detection model, which provides both pixel-wise segmentation and object localization within a single architecture. This allows for simultaneous identification and precise boundary delineation of the PP, contributing to enhanced clinical reliability in orthodontic and diagnostic applications.

In our study, the YOLOv8-seg model demonstrated high recall in detecting the PP in LCRs. This finding is consistent with prior research, which has indicated that earlier models, such as YOLOv4 and Faster R-CNN, face considerable challenges in attaining high recall rates, often resulting in increased instances of missed detections. For example, a comparative study examining the efficacy of various object detection models for Alzheimer's disease classification reported that YOLOv4 achieved a mean average precision (mAP) of 84%, while Faster R-CNN exhibited a significantly superior mAP of 99% [52]. For instance, a study comparing these models for Alzheimer's disease classification reported that YOLOv4 achieved a mean average precision (mAP) of 84%, while Faster R-CNN had a mAP of 99%; however, YOLOv4 exhibited better performance in certain classifications, particularly for moderate cases, suggesting variability in recall performance across different conditions [53]. Furthermore, another study focusing on weapon detection in surveillance videos found that YOLOv4 achieved a higher mAP score compared to Faster R-CNN, indicating its superior detection capabilities in that context [54]. These findings suggest that while YOLOv4 has demonstrated strong performance in specific applications, challenges in achieving consistently high recall rates across diverse medical imaging tasks remain, highlighting the potential advantages of models like YOLOv8-seg in improving detection performance [55]. Furthermore, its balance between precision and computational efficiency enhances its suitability for clinical applications, where both accuracy and processing speed are essential for patient care [46, 56]. The attributes of YOLOv8 thus position it as a promising technological advancement for real-time diagnostic tasks, potentially revolutionizing the landscape of medical imaging by minimizing missed diagnoses while ensuring that professionals can operate efficiently within demanding clinical settings [57]. These qualities contribute to the viability of YOLOv8-seg as a valuable tool in the ongoing evolution of diagnostic methodologies in orthodontics and other medical disciplines.

Moreover, the adjustment of the number of trainable parameters in the YOLOv8-seg model to align with the dataset size exemplifies a thoughtful approach to model optimization, which is essential for achieving robust performance in machine learning applications [58, 59]. This aspect of our methodology aligns with the recommendations from previous research advocating for tailored AI solutions that consider the specific characteristics of the datasets being utilized [31, 60]. The ability of the YOLOv8-seg model to perform effectively under varying conditions of image quality and anatomical clarity suggests that it could serve as a valuable tool in routine orthodontic practice, potentially leading to improved patient outcomes through more accurate diagnoses and treatment planning [61, 62].

The limitations of this study on the detection of the PP using the YOLOv8-seg model in LCRs are multifaceted and warrant careful consideration. Firstly, while the dataset size was predefined and specified in the Methods section, its limited diversity in anatomical variations and imaging conditions may affect the model's ability to generalize across diverse clinical scenarios. Although the YOLOv8-seg model demonstrated promising results, the accuracy and reliability of AI models often improve with larger and more diverse datasets that better reflect real-world applications [60, 63]. Expanding the dataset to incorporate a broader range of anatomical variations and imaging conditions could further enhance the model's robustness and clinical applicability. Another limitation of this study is the imbalance among the anatomical variation classes in the dataset. Specifically, the "absent" class was substantially overrepresented compared to the "partial" and "complete" classes. This class distribution reflects the nature of the retrospective clinical data and may have introduced a bias in model training, potentially affecting the generalizability and classification performance across less-represented categories. Although data augmentation techniques were employed to reduce this effect, future studies should consider more balanced sampling strategies or synthetic data generation methods to ensure more uniform representation of anatomical subgroups. Additionally, a key limitation of this study is that all images were obtained from a single center using only one imaging device. Variations in image acquisition settings, device types, and clinical protocols across different institutions could influence model performance. Future studies should consider multi-center datasets with images from different radiographic systems to improve generalizability. Another important consideration is the lack of comparison with a gold standard imaging modality such as Cone Beam Computed Tomography (CBCT). CBCT provides high-resolution, three-dimensional visualization of anatomical structures, which could offer a more objective reference for validating segmentation and

classification outcomes. However, due to the retrospective design of this study and the fact that lateral cephalograms are the standard imaging modality used in routine orthodontic evaluations, CBCT data were not available for the included cases. As a result, the performance of the YOLOv8-seg model could not be benchmarked against volumetric ground truth data. Future studies should incorporate CBCT or similar imaging modalities to enable more comprehensive validation of model accuracy and to better assess its diagnostic potential across multiple imaging platforms. Furthermore, the complexity of the anatomical structures surrounding the PP presents another challenge. As noted in previous research, the evaluation of cervical vertebrae on LCRs can be complicated by overlapping structures, which may obscure the visibility of the PP [60, 64]. This inherent difficulty in image interpretation could lead to misidentification or missed detections, thereby affecting the overall diagnostic accuracy of the AI model. The segmentation performance, while high, may still be susceptible to errors in cases where anatomical boundaries are not clearly defined, highlighting the need for further refinement of the model to enhance its robustness in challenging imaging conditions [64]. An analysis of misclassified cases revealed that incorrect predictions were primarily associated with anatomical variations and patient positioning differences. Variations in the morphology of the C1 cervical vertebra, as well as slight deviations in head positioning, led to partial visibility of key landmarks, which may have influenced the model's performance. To mitigate these limitations, future studies should consider expanding the dataset to include a broader range of anatomical variations and employing advanced data augmentation techniques to enhance model robustness. Additionally, this study used a predefined dataset split instead of k-fold cross-validation to maintain a balanced distribution across training, validation, and testing sets. While this approach provided stable performance estimation, future studies could implement k-fold cross-validation to further assess model robustness and reduce variability across different dataset partitions. Moreover, the reliance on a single AI model for detection may limit the comprehensiveness of the analysis. Different AI algorithms may exhibit varying strengths and weaknesses depending on the specific characteristics of the data and the task at hand [59, 65]. Future studies could benefit from a comparative analysis of multiple AI models—including not only different architectures (e.g., Faster R-CNN, EfficientDet) but also more recent versions of the YOLO series such as YOLOv12—to identify the most effective approach for PP detection and to ensure a more thorough exploration of AI capabilities in this context. Lastly, the interpretability of AI models remains a critical concern. Although the YOLOv8-seg model enables automated segmentation, the decision-making process of deep learning models remains largely opaque—often referred to as the 'black box' problem. This lack of interpretability may hinder clinical trust and adoption, emphasizing the need for explainable AI techniques to enhance transparency [66]. This lack of transparency may hinder clinicians' trust in AI-assisted diagnoses and their willingness to integrate such technologies into routine practice. Addressing these interpretability issues is essential for fostering confidence in AI applications within orthodontics and ensuring that practitioners can effectively utilize these tools in clinical decision-making.

Conclusion

In conclusion, this study successfully demonstrates the efficacy of the YOLOv8-seg model in the detection of the PP within lateral cephalometric radiographs, highlighting the transformative potential of artificial intelligence in orthodontic diagnostics. The model's high segmentation performance, evidenced by metrics such as 62.81% precision and 88.7% recall, underscores its ability to accurately identify this often-overlooked anatomical structure, even in challenging imaging conditions where boundaries may be unclear. By addressing the limitations of traditional diagnostic methods, this research not only contributes to the growing body of literature on AI applications in orthodontics but also sets a foundation for future advancements in automated cephalometric analysis. Integrating AI technologies like the YOLOv8-seg model into clinical practice has the potential to enhance diagnostic accuracy, optimize workflow efficiency, and significantly improve patient outcomes in orthodontic care.

Abbreviations

AI	Artificial Intelligence
BCE	Binary Cross Entropy
CBCT	Cone Beam Computed Tomography
CIoU	Complete Intersection over Union
CNN	Convolutional Neural Network
COCO	Common Objects in Context
CSP	Cross Stage Partial
CSPDarkNet53	Cross Stage Partial DarkNet-53
DFL	Distribution Focal Loss
F1	F1 Score
FN	False Negative
FP	False Positive
FPN	Feature Pyramid Network
IoU	Intersection over Union
LCR	Lateral Cephalometric Radiograph
mAP	Mean Average Precision
mAP50	Mean Average Precision at 0.50 IoU threshold
mAP95	Mean Average Precision at 0.50 to 0.95 IoU thresholds
NMS	Non-Maximum Suppression
PAN	Path Aggregation Network
PP	Ponticulus Posticus
TP	True Positive
VIA	VGG Image Annotator
YOLO	You Only Look Once
YOLOv8-seg	YOLO Version 8 with Segmentation Capability

Supplementary Information

The online version contains supplementary material available at https://doi.org/10.1186/s12903-025-06196-8.

Supplementary Material 1

Acknowledgements
Not applicable.

Author contributions
G.M. and M.A. were responsible for the study concept and design. G.M. performed the dataset preparation, model training, and initial manuscript drafting. M.A. contributed to data annotation and model evaluation. S.B. and M.C. assisted in statistical analysis and interpretation of the results. All authors participated in the manuscript revision, provided critical feedback, and approved the final version of the manuscript.

Funding
The authors declare that no funds, grants, or other support were received during the preparation of this manuscript.

Data availability
The datasets generated and/or analyzed during the current study are not publicly available due to institutional data privacy policies, but are available from the corresponding author on reasonable request.

Declarations

Ethics approval and consent to participate
All procedures performed in studies involving human participants were in accordance with the ethical standards of the institutional and/or national research committee and with the 1964 Helsinki Declaration and its later amendments or comparable ethical standards. The study was approved by Institutional Review Board of Dentistry Faculty, Necmettin Erbakan University (Approval No: 2023/308). Written informed consent was obtained from all participants.

Consent for publication
Not applicable.

Competing interests
The authors declare no competing interests.

Received: 10 February 2025 / Accepted: 19 May 2025
Published online: 28 May 2025

References

1. Pérez IE, Chávez AK, Ponce DJ. Frequency of ponticulus posticus in lateral cephalometric radiography of Peruvian patients. Int J Morphol. 2014;32(1).
2. Perić R, Krstonošić B, Starčević I. Morphometric study of the posterior arch of atlas vertebra in the Serbian population. Med Pregl. 2018;71(7–8):250–5.
3. Shetty AS, Jetti R, Sirasanagandla SR, Nelluri VJ. A case report of atlanto-occipital assimilation. Br J Med Surg. 2018;17(1):169.
4. Bayrakdar IS, Miloglu O, Altun O, Gumussoy I, Durna D, Yilmaz AB. Cone beam computed tomography imaging of ponticulus posticus: prevalence, characteristics, and a review of the literature. Oral Surg Oral Med Oral Pathol Oral Radiol. 2014;118(6):e210–9.
5. Natsis K, Piperaki ET, Fratzoglou M, Lazaridis N, Tsitsopoulos PP, Samolis A, et al. Atlas posterior arch and vertebral Artery's groove variants: a classification, morphometric study, clinical and surgical implications. Surg Radiol Anat. 2019;41:985–1001.
6. Keser N, Çıkla U, Özaydın B, Başkaya MJ. The importance of arcuate foramen, a variation of the atlas: a microsurgical cadaveric study and review of the literature. Int Med J. 2019;20(5).
7. Sharma V, Chaudhary D, Mitra R. Prevalence of ponticulus posticus in Indian orthodontic patients. J Dent Res. 2010;39(5):277–83.
8. Magat G, Akyuz M. A study evaluating the prevalence of the bony Bridge in the atlas posterior arch in a Turkish population. Gevher Nesibe J Med Health Sci. 2023;8(3):524–9.
9. Gasenzer ER, Kanat A, Ozdemir V, Neugebauer EJ. Analyzing of dark past and bright present of neurosurgical history with a picture of musicians. Br J Neurosurg. 2018;32(3):303–4.
10. Nishimoto S, Sotsuka Y, Kawai K, Ishise H, Kakibuchi M. Personal computer-based cephalometric landmark detection with deep learning, using cephalograms on the internet. J Craniofac Surg. 2019;30(1):91–5.
11. Breiman L. Statistical modeling: the two cultures (with comments and a rejoinder by the author). Stat Sci. 2001;16(3):199–231.
12. Yu H, Cho S, Kim M, Kim W, Kim J, Choi JJ. Automated skeletal classification with lateral cephalometry based on artificial intelligence. J Dent Res. 2020;99(3):249–56.
13. Kunz F, Stellzig-Eisenhauer A, Zeman F, Boldt J. Artificial intelligence in orthodontics. J Orofac Orthop. 2020;81(1):52–68.
14. Redmon J, Farhadi A. YOLO9000: Better, faster, stronger. In: Proceedings of the IEEE Conference on Computer Vision and Pattern Recognition (CVPR); 2017. pp. 6517–26.
15. Hussain M. YOLOv1 to V8: unveiling each variant– a comprehensive review of YOLO. IEEE Access. 2024;12:42816–33.
16. Lợi NK, Nguyen KD, Nguyen K. Real-time UAV-based vehicle detection: a comparative evaluation of YOLO models. Indian J Comput Sci Eng. 2023;14(6):902–11.
17. Dong J, Wang J, Lin H, Liu W. M-YOLOv8s: classification and identification of different microalgae species based on the improved YOLOv8s model for prevention of harmful algal blooms. ACS EST Water. 2024;5(1):329–40.
18. Shi J, Xiang M. Using ghost Convolution YOLO to detect brain tumor. Int J Imaging Syst Technol. 2024; [Epub ahead of print].
19. Han R, Liu X, Chen T. YOLO-SG: salience-guided detection of small objects in medical images. J Imaging. 2022; [Epub ahead of print].
20. Kaya E, Güneç HG, Gökyay S, Kutal S, Gülüm S, Ates HF. Proposing a CNN method for primary and permanent tooth detection and enumeration on pediatric dental radiographs. J Clin Pediatr Dent. 2022;46(4):293–8.
21. Hao Y, Zhu L, Wang X, Wang P, Hu W, Zeng Y et al. Improved detection and counting performance of microplastics in common carp whole blood by an attention-guided deep learning method. Sci Total Environ. 2022; [Epub ahead of print].
22. Zhu L, Geng X, Li Z, Liu C. Improving YOLOv5 with attention mechanism for detecting boulders from planetary images. Remote Sens. 2021;13(18):3776.
23. Mahasin M, Dewi IA. Comparison of CSPDarkNet53, CSPResNeXt-50, and EfficientNet-B0 backbones on YOLOv4 as object detector. Int J Eng Sci Inf Technol. 2022;2(3):64–72.
24. Bochkovskiy A, Wang CY, Liao HY. YOLOv4: optimal speed and accuracy of object detection. ArXiv. 2020; ArXiv:2004.10934.
25. Ju RY, Cai W. Fracture detection in pediatric wrist trauma X-ray images using YOLOv8 algorithm. Sci Rep. 2023;13(1):20077.
26. Guo J, Lou H, Chen H, Liu H, Gu J, Bi L, et al. A new detection algorithm for alien intrusion on highway. Sci Rep. 2023;13(1):10667.
27. Wang G, Chen Y, An P, Hong H, Hu J, Huang T. UAV-YOLOv8: a small-object-detection model based on improved YOLOv8 for UAV aerial photography scenarios. Sens (Basel). 2023;23(16):7190.
28. Zeng Q, Zhou G, Wan L, Wang L, Xuan G, Shao Y. Detection of coal and gangue based on improved YOLOv8. Sens (Basel). 2024;24(4):1246.
29. Bolya D, Zhou C, Xiao F, Lee YJ. YOLACT: real-time instance segmentation. In: Proceedings of the IEEE/CVF International Conference on Computer Vision (ICCV); 2019. pp. 9157–66.
30. Singarimbun RN, Nababan EB, Sitompul OS. Adaptive moment estimation to minimize square error in backpropagation algorithm. In: 2019 Int Conf Comput Sci Inf Technol (ICoSNIKOM). IEEE; 2019. pp. 1–7.
31. DiPalma G, Inchingolo AD, Inchingolo AM, Piras F, Carpentiere V, Garofoli G, et al. Artificial intelligence and its clinical applications in orthodontics: a systematic review. Diagnostics (Basel). 2023;13(24):3677.
32. Chalkoo AH. Cervical vertebral bone age Estimation and its correlation to chronological age. Int J Appl Dent Sci. 2022;8(4):113–6.
33. Hwang H, Moon JH, Kim M, Donatelli RE, Lee SJ. Evaluation of automated cephalometric analysis based on the latest deep learning method. Angle Orthod. 2021;91(3):329–35.
34. Palanivel N, G LP SD. B S, M SM. The Art of YOLOv8 algorithm in cancer diagnosis using medical imaging. Int J Health Sci. 2023; [Epub ahead of print].
35. Widayani A, Putra AM, Maghriebi AR, Adi DZC, Ridho MHF. Review of application YOLOv8 in medical imaging. Indones Appl Phys Lett. 2024;5(1):23–33.

36. Huang C, Yang D, Zhang X. Lightweight object detection algorithm for road scenes based on YOLOv8. Sens (Basel). 2024; [Epub ahead of print].
37. Wang P, Deng H, Guo J, Ji S, Meng D, Bao J et al. Leaf segmentation using modified YOLOv8-seg models. Life (Basel). 2024;14(6): [Epub ahead of print].
38. Su Y, Qiu Z, Huang X, Lu D. Enhanced YOLOv8 algorithm for large-scale multi-object detection and its application in defect detection in power systems. In: Eighth International Conference on Energy System, Electricity, and Power (ESEP 2023); 2024. SPIE; pp. 2094–9.
39. Liu S, Qi L, Qin H, Shi J, Jia J. Path aggregation network for instance segmentation. In: 2018 IEEE/CVF Conference on Computer Vision and Pattern Recognition (CVPR); 2018. pp. 8759–68.
40. Jocher G, Chaurasia A, Qiu J, Stoken A. YOLOv8 documentation. Ultralytics. 2023. Available from: https://docs.ultralytics.com
41. Shorten C, Khoshgoftaar TM. A survey on image data augmentation for deep learning. J Big Data. 2019;6(1):60.
42. Tan M, Le Q. EfficientNet: rethinking model scaling for convolutional neural networks. In: Proceedings of the 36th International Conference on Machine Learning (ICML); 2019. pp. 6105–14.
43. Vaikunth M, Dejey D, Vishaal C, Balamurali S. Optimizing helmet detection with hybrid YOLO pipelines: a detailed analysis. Int J Comput Appl. 2024; [Epub ahead of print]:83–93.
44. Murthy A, Dsouza O. A review of crown detection in Yakshagana images using CNN algorithm. Int Res J Mod Eng Technol Sci. 2023; [Epub ahead of print].
45. Fu L, Yang Z, Wu F, Zou X, Lin J, Cao Y, et al. YOLO-Banana: a lightweight neural network for rapid detection of banana bunches and stalks in the natural environment. Agronomy. 2022;12(2):391.
46. Khanagar S, Al-Ehaideb A, Maganur PC, Vishwanathaiah S, Patil S, Baeshen HA, et al. Developments, application, and performance of artificial intelligence in dentistry– a systematic review. J Dent Sci. 2021;16(1):508–22.
47. Aseil Nadhum K, Aseel Nadhum K. Literature survey on YOLO models for face recognition in COVID-19 pandemic. J Image Process Intell Remote Sens. 2023;3(4):27–35.
48. Shah U, Khan S, Alzubaidi M, Agus M, Househ M. Unveiling the potential of ChatGPT and YOLOv7 for evaluating children's emotions using their artistic expressions. J Innov Health Inf. 2024; [Epub ahead of print].
49. Langius-Wiffen E, de Jong PA, Hoesein FAM, Dekker L, van Hove AF, Nijholt IM et al. Retrospective batch analysis to evaluate the diagnostic accuracy of a clinically deployed AI algorithm for the detection of acute pulmonary embolism on CTPA. Insights Imaging. 2023;14(1).
50. Zhao T, Zhou J, Yan J, Cao L, Cao Y, Hua F, et al. Automated adenoid hypertrophy assessment with lateral cephalometry in children based on artificial intelligence. Diagnostics (Basel). 2021;11(8):1386.
51. Lee KS, Ryu JJ, Jang HS, Lee DH, Jung SK. Deep convolutional neural networks based analysis of cephalometric radiographs for differential diagnosis of orthognathic surgery indications. Appl Sci. 2020;10(6):2124.
52. Thanathornwong B, Suebnukarn S. Automatic detection of periodontal compromised teeth in digital panoramic radiographs using faster regional convolutional neural networks. Imaging Sci Dent. 2020;50(2):169–74.
53. Mirchandani R, Yoon C, Prakash S, Khaire A, Naran A, Nair A et al. Comparing the architecture and performance of AlexNet, Faster R-CNN, and YOLOv4 in the multiclass classification of Alzheimer brain MRI scans. In: Proceedings of the International Conference on Medical Imaging and Computer-Aided Diagnosis (MICAD); 2023. p. [Epub ahead of print].
54. Vijayakumar KP, Pradeep K, Balasundaram A, Dhande A. R-CNN and YOLOv4 based deep learning model for intelligent detection of weaponries in real-time video. Math Biosci Eng. 2023;20(12):21611–25.
55. Wong KF, Lam XY, Jiang Y, Yeung AWK, Lin Y. Artificial intelligence in orthodontics and orthognathic surgery: a bibliometric analysis of the 100 most-cited articles. Head Face Med. 2023;19(1).
56. Ahmed N, Abbasi MS, Zuberi F, Qamar W, Halim MS, Maqsood A, et al. Artificial intelligence techniques: analysis, application, and outcome in dentistry—A systematic review. Biomed Res Int. 2021;2021:1–15.
57. Xu L, Mao X, Sun M, Liu W, Wang Y, Tang Y. Lung lesions detection from CT images based on the modified Faster R-CNN. In: 2020 International Conference on Computer, Information and Telecommunication Systems (CITS); 2020. pp. 1–5.
58. Subramanian AK, Chen Y, Almalki A, Sivamurthy G, Kafle D. Cephalometric analysis in orthodontics using artificial intelligence—A comprehensive review. Biomed Res Int. 2022;2022:1–9.
59. Monill-González A, Rovira-Calatayud L, d'Oliveira NG, Ustrell-Torrent JM. Artificial intelligence in orthodontics: where are we now? A scoping review. Orthod Craniofac Res. 2021;24(S2):6–15.
60. Zhou J, Zhou H, Pu L, Gao Y, Tang Z, Yang Y, et al. Development of an artificial intelligence system for the automatic evaluation of cervical vertebral maturation status. Diagnostics (Basel). 2021;11(12):2200.
61. El-Dawlatly MM, Attia K, Abdelghaffar A, Mostafa YA, El-Ghafour MA. Preciseness of artificial intelligence for lateral cephalometric measurements. J Orofac Orthop. 2023;85(S1):27–33.
62. Bonny T, Al Nassan W, Obaideen K, Al Mallahi MN, Mohammad Y, El-damanhoury HM. Contemporary role and applications of artificial intelligence in dentistry. F1000Res. 2023;12:1179.
63. Le VNT, Kang J, Oh IS, Kim JG, Yang YM, Lee D. Effectiveness of human–artificial intelligence collaboration in cephalometric landmark detection. J Pers Med. 2022;12(3):387.
64. Seo H, Jeong TS, Shin J. Comparison of deep learning models for cervical vertebral maturation stage classification on lateral cephalometric radiographs. J Clin Med. 2021;10(16):3591.
65. Khanagar S, Al-Ehaideb A, Vishwanathaiah S, Maganur PC, Patil S, Naik S, et al. Scope and performance of artificial intelligence technology in orthodontic diagnosis, treatment planning, and clinical decision-making– a systematic review. J Dent Sci. 2021;16(1):482–92.
66. Real AD, Real OD, Sardiña S, Oyonarte R. Use of automated artificial intelligence to predict the need for orthodontic extractions. Korean J Orthod. 2022;52(2):102–11.

Publisher's note